Application of the Johnson-Cook plasticity model in the Finite Element simulations of the nanoindentation of the cortical bone

Djamel Remache, Marie Semaan, Jean-Marie Rossi, Martine Pithioux, Jean-Louis Milan

Application of the Johnson-Cook plasticity model in the Finite Element simulations of the nanoindentation of the cortical bone.

D. Remache[a,b], M. Semaan[a,b,c], J.M Rossi[b,d], M. Pithioux[a,b], J.L Milan[a,b]

[a] *Aix Marseille Univ, CNRS, ISM, Marseille, France,*
[b] *Aix Marseille Univ, APHM, CNRS, ISM, Sainte-Marguerite Hospital, Institute for Locomotion, Department of Orthopaedics and Traumatology, Marseille, France*
[c] *University of Balamand, Faculty of Engineering, Al Kurah, Lebanon*
[d] *Aix Marseille Univ, CNRS, Centrale Marseille, ISM, Marseille, France*

Abstract

The mechanical behavior of the cortical bone in nanoindentation is a complicated mechanical problem. The finite element analysis has commonly been assumed to be the most appropriate approach to this issue. One significant problem in nanoindentation modeling of the elastic–plastic materials is pile-up deformation, which is not observed in cortical bone nanoindentation testing. This phenomenon depends on the work-hardening of materials; it doesn't occur for work-hardening materials, which suggests that the cortical bone could be considered as a work-hardening material. Furthermore, in a recent study [59], a plastic hardening until failure was observed on the micro-scale of a dry ovine osteonal bone samples subjected to micropillar compression. The purpose of the current study was to apply an isotropic hardening model in the finite element simulations of the nanoindentation of the cortical bone to predict its mechanical behavior. The Johnson–Cook (JC) model was chosen as the constitutive model. The finite element modeling in combination with numerical optimization was used to identify the unknown material constants and then the finite element solutions were compared to the experimental results. A good agreement of the numerical curves with the target loading curves was found and no pile-up was predicted. A Design Of Experiments (DOE) approach was performed to evaluate the linear effects of the material constants on the mechanical response of the material. The strain hardening modulus and the strain hardening exponent were the most influential parameters. While a positive effect was noticed with the Young's modulus, the initial yield stress and the strain hardening modulus, an opposite

effect was found with the Poisson's ratio and the strain hardening exponent. Finally, the JC model showed a good capability to describe the elastoplastic behavior of the cortical bone.

Keywords: Mechanical cortical bone behavior, Nanoindentation test, Inverse optimization approach, Design of experiments (DOE), Johnson-Cook model

1. Introduction

The instrumented indentation technique is usually performed for local mechanical characterization of the cortical bone [12, 13, 21, 23, 24, 25, 27, 34, 38, 55, 56, 63, 69, 72]. The well documented Oliver-Pharr (OP) analytical approach [47, 48], available in the software included with most commercial Indentation Testers, has widely been adopted for measuring the elastic modulus and the hardness of materials from indentation load–displacement data obtained during one cycle of loading and unloading. This method has been introduced according to assumptions that the material is homogeneous, linearly elastic, isotropic and incompressible, and during unloading, it is assumed that only the elastic displacements are recovered, i.e., the unloading response is considered as purely elastic [15, 47, 50]. This method is therefore limited with regard to determining the mechanical properties of the heterogeneous and multi-scale structural materials such as the cortical bone tissue [28, 30]. Indeed, in addition to the inhomogeneities of the material, such as porosity, defects, grain boundaries, etc..., viscoplastic deformations are added to the elastic deformation [7, 12, 13, 23, 24, 26, 33, 41, 49, 64, 68, 76], making the strain field induced under the indenter very heterogeneous and complex. Furthermore, the mechanical properties of the cortical bone depend also on other factors such as the anatomical zone of the tested sample, sex, age, the hydration state of the material, the probe geometry, etc...[25, 33, 45, 49, 58]. The finite element approach has thus become essential for determining the mechanical properties of materials such as the cortical bone [8, 12, 22], particularly their time-dependent mechanical properties such as creep, viscoelasticity or elastoplasticity [12, 14].

*

Email addresses: djamel.remache@univ-amu.fr (D. Remache), marie.semaan@balamand.edu.lb (M. Semaan), jean-marie.rossi@centrale-marseille.fr (J.M Rossi), martine.pithioux@univ-amu.fr (M. Pithioux), jean-louis.milan@univ-amu.fr (J.L Milan)

One significant problem in the indentation modeling of the elastic–plastic materials is the pile-up of material around the contact impression, due to a plastic flow of material from beneath the indenter toward the sample surface. This phenomenon is frequently observed in the indentation of the elastic-perfectly-plastic materials such as metal materials [22], but it doesn't occur in the indentation of work-hardening materials [9]. Based on Atomic Force Microscopy [22, 43, 61] and Scanning Electron Microscopy [37] observations and based on a statistical shape modeling of the indentation residual imprint [61], it was observed that pile-up doesn't occur in cortical bone tissue during the nanoindentation testing, which suggests that the material could be considered as a work-hardening material. It would then be appropriate to use a plastic hardening model for the finite element modeling of the nanoindentation of the cortical bone tissue. Indeed, the classical metal plasticity model predicted a significant pile-up of material and an overestimation of the maximum depth by approximately 30% [43], however, it has been suggested by [22] that it might be possible to eliminate the pile-up effect by introducing a strain hardening rate to the classical metal plasticity model [9, 22, 43]. The finite element results of this study have not been validated by comparison with the experimental results. In a recent study [59], a dry ovine osteonal bone was subjected to micropillar compression, microindentation and macroscopic compression tests to identify the elastic modulus, yield stress, plastic deformation, damage accumulation and failure mechanisms. The results showed that, on the micro-scale a highly ductile behavior with continuous hardening and no damage until failure were exhibited by the samples, whereas, on the macro-scale the samples failed mostly in a quasi-brittle fashion due to the existing of cracks, pores and defects leading to a reduction of strength and ductility. The measured strength on the micro-scale was found to be higher than on the macro-scale. It was assumed that on the micro-scale the indentation results represent the local bulk material properties. In a more recent study [52], nanoindentation was performed on mouse femur and then Focused Ion Beam-Scanning Electron Microscopy (FIB-SEM) was used to map microporosities below the nanoindentation sites. Several cavities such as lacunae were identified, but for the majority of indentation sites, cavity-free material was found, and this corresponded to a reasonable consistency in the maximum indentation depth and Young's modulus. A significantly softer response was measured in the sites with subsurface cavities. Further

investigations [52, 60, 61], based on the porous nature of the cortical bone, assumed that a model, which accounts for frictional mechanisms, is required for accurate material behavior prediction [12, 13, 43, 66]. The extended Drucker-Prager plasticity model [19], intended for geological materials that exhibit pressure-dependent yield, has accurately predicted the post-yield behavior of a cortical bone and no pile-up in the material [43]. However, no evidence of fracture events was observed in the experimental testing, as it has been expected.

In the current study, nanoindentation tests were performed on a human femur cortical bone. Thanks to the microscope included with the used commercial Indentation Tester, visible surface defects, holes, and pores were avoided. Hence, it was assumed that the nanoindentation results represent the local bulk material properties. The cortical bone was considered as a work-hardening elastic-plastic material. The Johnson–Cook (JC) isotropic hardening model [36] was chosen as the constitutive model. Unlike the most previous studies, we were interested in the elastic–plastic response during the loading phase of a cortical bone sample subjected to nanoindentation. To minimize errors that might result from underestimating of the contact area, the elastic constants, corresponding to the initial elastic contact, and the JC material constants were identified from the non-linear curve-fit of the force-displacement raw data using an inverse analysis. The elastic constants were predicted independently and simultaneously unlike in the OP method, which requires a priori knowledge of one constant to compute the second one. The finite element method in combination with numerical optimization were used to identify the unknown material parameters. This indentation data analysis method has already been used to investigate some classical materials such as polymer layers [15, 16] and steel [39].

2. Materials and Methods

2.1. Experimental tests

A cortical bone sample was obtained from the femur of a human female cadaver (82 years old) without bone disease. The sample was cut into a parallelepiped shape of a few millimeters by a water-cooled low-speed diamond saw (Buehler Isomet 4000, Buehler, Lake Bluff, IL, USA) and was stored at -20°C. No chemicals were used for cleaning and

dehydration in order to preserve the mechanical properties of the material microstructural features [53]. Also, resin was avoided since its infiltration will alter the measured elastic properties [10]. The sample sides were polished using silicon carbide abrasive papers of decreasing grit size (400, 800 and 1200 grit) under deionized water [56, 55] then, with a diamond suspension (1 µm). The sample was cleaned of polishing dust with water.

Nanoindentation tests were conducted at room temperature (∼23°C) using an indentation Tester of Anton Paar (Tester NHT^2, Switzerland and Austria) with the modified Berkovich diamond tip. The tip area function was calibrated by a fused silica reference sample. The tests were performed in the load control mode in the two principal bone directions, i.e., the axial direction (corresponding to the long bone axis) and the transverse direction (perpendicular to the long bone axis). In the axial direction, the tests were performed at two locations; osteons and interstitial lamellae observed by optical microscopy (Fig. 1). In the transverse direction, it was difficult to distinguish between osteons and interstitial lamellae. The nanoindentation tests were conducted up to a maximum load of 20 mN, at a loading/unloading rate of 40 mN/min. A total of 26 indents were made: 8 in osteons locations, 8 in interstitial lamellae locations, and 10 in the transversal side.

The elastic modulus and the hardness constant of the cortical bone sample were measured by the OP technique [47, 48], available in the software included with the commercial Indentation Tester. The elastic modulus is given by:

$$E = \frac{1-\nu^2}{\frac{1}{E_r} - \frac{1-\nu_i^2}{E_i}} \tag{1}$$

where E_i is Young's modulus of the indenter (E_i=1141 GPa), ν_i (ν_i=0.07) and ν are Poisson's ratio of the indenter and the material, respectively, and E_r is the reduced elastic modulus given by:

$$E_r = \frac{S.\sqrt{\pi}}{2.\beta.\sqrt{A\,(h_c)}} \tag{2}$$

where $S = dF/dh$ is the contact stiffness (defined as the slope of the initial part of the unloading curve during the first stage of unloading), A is the projected area of the contact impression, β is a constant (a correction factor) which depends on the indenter geometry [56] (for the Berkovich indenter $\beta = 1.034$), h_c is the contact depth of the indenter with

the sample at the maximum indentation force. A value of 0.3 was chosen for ν.

The hardness, H, is given by the following relationship:

$$H = \frac{P_{max}}{A} \tag{3}$$

where P_{max} is the maximum indentation force.

2.2. Finite Element analysis

2.2.1. Finite element model

The numerical simulation of the Berkovich indentation experiments was modeled in two-dimensional axisymmetric finite element model using the commercial finite element code Abaqus® 6.14-2. A rectangular region of dimensions 40×40 μm was assumed as the problem domain. The Berkovich indenter was defined as an analytical rigid surface part with an angle of 65.27° between the vertical axis and the indenter face, and the cortical bone was assumed to be a deformable body. Asymmetric linear triangular elements of type CAX3 were used for meshing the sample geometry (total number of elements: 5202 and total number of nodes: 2704). After mesh convergence study, finer elements were used in the vicinity of the indenter surface and coarse elements farther away. A reference point was defined on the indenter geometry, on which a total indentation load of 20 mN was applied under load-control conditions. The geometry and boundary conditions of the finite element model are illustrated in Fig. 2. The indenter was defined as master surface, while the nodes at the top of the sample part were defined as slave surface. A surface-to-surface (standard) contact using the finite-sliding formulation was defined as a type of interaction, and to avoid the penetration of the slave surface into the master surface at the constraint locations, the "hard" contact was chosen as a contact property. A rigid body constraint was applied to the indenter and a frictionless hard contact was assumed. The elastic-plastic behavior of the material was governed by the Johnson-Cook behavior law presented in the following section.

2.2.2. Johnson-Cook constitutive model

The nanoindentation tests were simulated using the isotropic hardening model proposed by Johnson–Cook (JC) [36]. The JC model is a phenomenological model for

materials subjected to large strains, high strain rates and high temperatures. The flow stress of this particular type of Mises plasticity model is expressed as:

$$\sigma = \left[A + B\varepsilon_p^n\right]\left[1 + C\ln\left(\frac{\dot{\varepsilon}}{\dot{\varepsilon}_0}\right)\right]\left[1 - T^{*m}\right] \tag{4}$$

$$T^* = \frac{T - T_0}{T_m - T_0}$$

where A , B, n, C, and m are the material constants; ε_p is the equivalent plastic strain, $\dot{\varepsilon}$ and $\dot{\varepsilon_0}$ are the plastic strain rate and the reference plastic strain rate (i.e., which corresponds to the quasi-static test), respectively. T^* is the normalized temperature; T_0 is a reference (or transition) temperature (i.e., the room temperature in a quasi-static test), and T_m is the melting temperature. A is defined as the initial static yield stress (i.e., $\sigma = A$ when $\varepsilon_p = 0$,$\dot{\varepsilon}$=$\dot{\varepsilon_0}$ and $T = T_0$); B is the strain hardening modulus and n is the strain hardening exponent.

The expression in the first set of brackets gives the stress as a function of strain for $\dot{\varepsilon} = \dot{\varepsilon_0}$ and $T^* = 0$. The expressions in the second and third sets of brackets represent the effects of elevated strain rates and temperature, respectively. Since the experimental indentation was a quasi-static test without significant thermal changes, the second and third factor in the constitutive relationship were neglected. Therefore, we had to determine the constants in the first set of brackets. Finally, the model was used in conjunction with a linear elastic material model. The choice of this model was based on the fact that it is able to describe the strain hardening effect in materials and because of its good prediction and simplicity [18]. This model was used in bone cutting simulations [2, 3, 1, 75] and in simulations of impact and penetration related problems [4].

2.3. Calibration procedure

Numerical optimization is a mathematical formulation that allows to minimize or maximize a particular objective function subjected to constraints on its variables [44]. The objective function depends on certain variables called unknowns or parameters (frequency, stress, displacement, material parameter...). So, in the optimization process, the objective, the variables, and the constraint functions are to be defined. In this

work, our goal was to determine the cortical bone constants so that the numerical force-displacement curve matches the experimental one. The force-displacement raw data were used in the inverse analysis as input data in order to minimize errors that might result from underestimating of the contact area. It was assumed that the measurement indentation errors accumulated during the loading phase such as, e.g. errors derived from friction, surface roughness or the material inhomogeneities are involved in the experimental raw data [15, 16].

The parameters identification procedure was developed combining the FEM code Abaqus® with HyperStudy® software, which is a multi-disciplinary design exploration software in Altair® HyperWorks®. The software uses mathematical approaches such as design of experiments (DOE), optimization, and stochastic studies. Each approach serves a different purpose in the design study. In this study, the optimization approach was used for calibration and the DOE was used for sensitivity analysis.

The calibration procedure is illustrated in Fig. 3. The procedure can be described in the following steps: (1) the finite element model was developed in Abaqus®(See section 2.2.1) and, then the Abaqus® input file was imported in HyperStudy® as well as the experimental force-displacement data. The numerical force-displacement history is extracted from the Abaqus® output database file. Since the indenter was load-controlled, the displacement is predicted. Abaqus® was specified as a solver in HyperStudy®. (2) the material constants were defined as design variables and the parameterization of the FE model was performed in HyperStudy®. The initial guess values assigned to the unknown design variables and their lower and upper boundaries are shown in Table 1. The upper bounds of the elastic modulus, the Poison's ratio and the initial yield stress were set according to their maximum values reported in the literature [5, 11, 17, 23, 55]. The upper bound of B was arbitrary chosen and the one of n is its maximum theoretical value. The initial values were taken from [2] (see Table 3), which is the only study that used the Johnson Cook model for modeling, except for the initial value of n, an average value with respect to its theoretical range of values [0;1] has been chosen because we found that the reported value (n=0.08) is very close to that of the perfectly plastic solid (i.e., n=0) such as metal. The lower bounds were arbitrary chosen. (3) for the calibration process, a response has to be defined as an objective function required to be minimized

in the optimization process. The curve_difference function was defined as the objective function. The curve_difference function is an HyperMath® function that calculates the integral of the absolute value of the difference between two curves over the common domain of the supplied functions. The curve_difference function is expressed as:

$$\int_a^b |f(x) - g(x)|\, dx \tag{5}$$

(4) in the optimization approach, the system identification procedure was used as the optimization problem formulation to minimize the objective function. This procedure consists to fit a set of responses to a set of target values by modifying a set of variables. In the case of the current study, the numerical curve was fitted to the experimental curve by modifying the material constants using a least squares formula described as:

$$\min \sum \left(\frac{f_i - \bar{f}_i}{\bar{f}_i} \right)^2 \tag{6}$$

where $\bar{f}_i$ response is the target value of the i^{th} response, and where the target values are the experimental data.

In the optimization step, several iterations are performed. During each iteration, the optimization algorithm updates the parameter values of the FE model until the optimal values are obtained. Several optimization methods are used by HyperStudy® such as Adaptive Response Surface Method (ARSM), Global Response Surface Method (GRSM), Sequential Quadratic Programming (SQP), etc....In this study, SQP was used for the objective optimization. SQP is a gradient-based iterative optimization method. For further details about this approach, see [44].

2.4. Design Of Experiments (DOE)

DOE is a mathematical approach developed to investigate the relationships between the different input variables of a design problem which influence the output responses [29, 67]. The DOE process available in Altair HyperStudy® was used to determine which material constants are most influential on the material responses to nanoindentation stress. The elastic (E and ν) and JC material constants were selected as design variables in the DOE process and the maximum equivalent stress as the material response. A DEO of type full factorial was used in this study. The full factorial DOE evaluates all

Table 1: Initial guess values and the lower and upper boundaries of the design variables in the optimization process. E_0 is the measured elastic modulus corresponding to each experimental test.

variable name	Lower Bound	Initial	Upper Bound
E (GPa)	15	20	30
ν	0.01	0.3	0.5
A(GPa)	0.01	0.05	0.12
B (GPa)	0.01	0.1	5
n	0.01	0.5	1

linear effects and interactions between the different design variables. The linear effect is evaluated by calculating the averaged responses at the lower and upper bounds of the design variables (given by Table 1 for the current study) and then plotted by drawing a straight line between the two average values corresponding to each design variable. The linear effect value of each design variable corresponds to the difference between its average responses. In the plot format, the effect is larger as the line becomes more vertical. A positive slope indicates a positive effect, ie., if a variable increases the response will also increase. In the full factorial DOE, the responses are evaluated for all combinations of design variable levels. The total number of runs of the full factorial DOE is given by this relationship: L^v, where L is the number of level studies, which corresponds to the number of bounds, and v the number of variables. For the current study, we have five variables and two-level studies (ie., for the lower bound and for the upper bound). The total number of runs of the full factorial DOE is then 32 runs, 16 runs for each bound value.

3. Results and Discussion

3.1. Experimental results

The average values of the experimental indentation moduli and hardnesses are summarized in Table 2. These values, obtained with the OP approach available in the software included with the commercial Indentation Tester, are within the range of values reported in previous studies for the same approach [33, 55, 62, 65]. A minimum difference of 4.6 GPa was found between the average values of the elastic modulus in the axial and

Table 2: The average values of the experimental nanoindentation moduli and hardnesses and their standard mean deviations of human cortical bone compared to some values found in the literature. In parentheses, is shown the number of indentations.

	Direction	Axial (in O.R)	Axial (in I.R)	Transverse
Current Study	E (GPa)	22.13±0.74 (8)	23.9±1.18 (8)	17.45± 0.47 (10)
	H(GPa)	0.72±0.05 (8)	0.83±0.10 (8)	0.63±0.05 (10)
[55](1)	E (GPa)	22.4±1.20 (72)	25.7±1.00 (58)	16.6±0.74 (58)
	H(GPa)	0.617±0.039 (72)	0.736±0.044 (58)	0.564±0.034 (58)
[33](2)	E (GPa)	18.6±4.2	20.3±5.1	NR
	H(GPa)	0.52±0.15	0.59±0.2	NR
[77](3)	E (GPa)	19.1 ±5.4	21.2 ±5.3	NR

O.R: Osteonal Region. I.R: Interstitial Region. NR = not reported. (1) tibiae cortical bone samples of two male humans (ages of 60 and 66). (2) femoral diaphysis cortical bone samples of four human subjects (males: age 53 and 77; females: age 77 and 93). (3) femoral diaphysis cortical bone samples of four females and four males (age: from 53 to 93 yr old).

transverse directions. Fig. 4 shows an example of the force-displacement curves corresponding to the axial and transverse directions. The curves show that the mechanical response of the cortical bone to nanoindentation depends on the loading direction, as found in the literature [12, 28, 69, 65]. The axial direction was found to be the stiffest bone direction while the interstitial lamellae were found to be stiffer than the osteons lamellae, as reported by [24, 33, 55, 56, 54, 69, 77]. For the same site, a scatter in nanoindentation results was observed [21, 54]. Fig. 5 provides an illustration of scatter in the nanoindentation results of the interstitial bone site. A deviation of 2.36 GPa in elastic modulus was found between its minimum value and maximum value. This deviation corresponds to a deviation of 122 nm in depth. This difference was 1.48 GPa in osteons site.

3.2. Numerical results

As mentioned in the introduction, one significant problem in nanoindentation modeling of the elastic-plastic materials is pile-up deformations. This phenomenon doesn't occur in work-hardening materials [9] and is not produced in cortical bone, as an elastic-plastic material [22, 37, 43]. The cortical bone was then considered as a work-hardening

elastic-plastic material. The purpose of this study was to apply a plastic hardening model to predict the mechanical behavior of the cortical bone in nanoindentation. The Johnson–Cook isotropic hardening model was chosen as the constitutive model. The finite element analysis was performed to solve the nanoindentation mechanical problem. With this approach, it was expected to predict simultaneously: no pile-up of material, the force-displacement curve of the nanoindentation test and realistic yield stress values, ie, which should be in agreement with those reported in the literature. To the best of our knowledge, this study is the first one that used an isotropic hardening model in simulations of the nanoindentation testing of bone.

The mean values of the elastic (E and ν) and the JC cortical bone constants determined by the inverse analysis are summarized in Table 3. To illustrate the results, the finite element modeling of the nanoindentation test was performed using the identified constants. Fig. 6 shows a representative example of the fit between the experimental and the predicted curves. As we can see from this figure, the numerical curve matches well with the experimental one. Fig. 7 shows an example of the finite element modeling of the nanoindentation testing. The equivalent plastic strain (PEEQ) contours within the cortical bone sample indicates important plastic strains beneath the indenter and shows that the stress region is located far away from the boundaries, which suggests that the considered problem domain was enough for the numerical simulation of the nanoindentation testing. The figure also shows that there is no obvious pile-up of material around the contact impression, which is characterized by an upward vertical displacement of the outer boundary of the contact area for Berkovich indenters [9, 12, 48]. This agrees with the bone experimental results [22, 37, 43]. Another result, the predicted mean values of the initial yield stress, A, lie within the range of values [0.04-0.12] GPa, reported in the literature [2, 5, 17]. The results presented thus far provide evidence that the JC model can predict accurately the elastoplastic behavior of the cortical bone. However, it would be noted that Table 3 shows a difference of about 0.5 GPa between the predicted and the corresponding measured mean values of the elastic modulus (Table 2). This difference can be due to the applied data analysis method [58], i.e., the proposed analysis method and the OP method. Indeed, the predicted elastic modulus was determined from the initial elastic contact and the experimental one was determined from the elastic response

Table 3: Mean values and standard mean deviations of the elastic and the JC cortical bone constants identified by the inverse analysis.

Direction	E (GPa)	ν	A (GPa)	B (GPa)	n
Axial (in O.R)	21.90±0.45	0.29±0,10	0.091±0,025	1.63±0.48	0.43±0.04
Axial (in I.R)	23.07±1.98	0.38±0,06	0.094±0.007	1.29±0.19	0.34±0.13
Transverse	18.27±1.28	0.44±0,04	0.043±0.033	1.77±0.30	0.52±0.07
[2]	20	-	0.05	0.1	0.08

O.R: Osteonal Region. I.R: Interstitial Region.

of the maximum contact area, beneath which a plastic straining was produced. On the other hand, unlike the OP method, which requires a priori knowledge of Poisson's ratio to compute the elastic modulus (equation 1), the proposed method allows to predict both the elastic constants independently and simultaneously. Previous investigation has proposed to decouple the elastic constants (E and ν) by using two different indenters to achieve accurate measurements [50]. The reported difference in elastic modulus can also be related to errors in Poisson's ratio fixed in the experimental testing [50, 32], Poisson's ratio was fixed at 0.3 in the experimental testing while its predicted mean values varied from 0.28 to 0.48, which is in good agreement with other studies [17]. Fig. 8 provides an illustration of the variation in the force as a function of the displacement for two different values of Poisson's ratio. This variation (of about of 2.5 mN) corresponded to an overestimation of the elastic modulus of about 1 GPa. Finally, the predicted JC constants were found to be elevated compared to those obtained from the tensile testing of the cortical bone by [2] (Table 3).

Linear effects of the elastic-plastic constants on the material response were evaluated using the full factorial DOE. The maximum equivalent stress was considered as the material response. Linear effects are shown in plot format in Fig. 9. For each material constant, the average response value is calculated for 16 runs of the full factorial DOE when the constant is at its lower bound value and 16 runs when the constant is at its upper bound value (see Table 1). The average values are indicated by the ends of the lines. The difference between the two average values, that is the linear effect value, is indicated in the legend. For example, for the lower bound of Young's modulus (15 GPa), an average maximum equivalent stress of 1.835 GPa was calculated for 16 results, whose

minimal value was 0.015 GPa and the maximum value was 5.116 GPa. For its upper bound (30 GPa), an average maximum equivalent stress of 1.905 GPa was calculated for 16 results, whose minimal value was 0.0163 GPa and maximum value was 5.122 GPa. The deducted linear effect value was then 0.069 GPa. As the figure shows, the Young's modulus, E, the strain hardening modulus, B, and the initial yield stress, A, have a positive effect and the Poisson's ratio, ν, and the strain hardening exponent, n, have a negative effect, which means an inverse effect on results, i.e., the maximum equivalent stress decreases when n increases [42]. Comparing the linear effect values displayed in the legends, and going from the least influence to the most influence on the material response within the current lower and upper boundaries, the parameters can be sorted as: E, A, ν, n, B. It is important to note that the order of the influence of the constants depends on the lower and upper boundaries.

As the full factorial DOE analysis has shown, the strain hardening modulus and the strain hardening exponent were the most influential parameters on the material response to nanoindentation stress. Thus, the stiffest bone region corresponded to the lowest magnitude of B and n. The strain hardening exponent measures the strain hardening ability of materials [11]. A perfectly elastic-plastic solid has a value of n=0. A mean values of n lying between 0.3 to 0.6 were predicted for the cortical bone. This ability of the cortical bone to strain-harden is probably due to its complex hierarchical structure, in particular its inorganic phase (33-43% bone volume) [30], whose the volume fraction varies with the indentation site and even with the single lamella. Indeed, the cortical bone is a dense connective tissue consisting of dense and hard concentric layers called lamellae [31, 57]. Each single lamella consists of mineralized collagen fibrils, a soft and ductile collagen fibrils reinforced with stiff hydroxyapatite crystals [35, 40, 70]. In each single lamella, the mineralized collagen fibrils, considered as the primary building block of bone [30], are oriented in one direction and rotate relative to the adjacent lamella [73]. So, it has been suggested that the local material response depends mainly on the mineral volume fraction and the fibrils arrangement [20, 28, 30, 45, 51]. A strengthening of the material could occur at the mineralized collagen fibrils level as a function of the tip penetration. Indeed, nanoindentation tests performed on hydroxyapatite single crystal revealed a nanoscale plasticity in the form of pile-up along the edges of the indenter [71],

which may induce a uniform increase of the yield stress as the indenter penetrates the material. In a recent study, it was shown that a highly ductile behavior with continuous hardening until failure was observed on the micro-scale of a dry ovine osteonal bone samples subjected to micropillar compression [59]. The material strengthening could also occur because of lamellae dislocation through slip [59] as it has been found in metals (e.g., dislocations pile-up at grain boundaries [11]). In contrast to these findings, a further study suggested that other parameters could affect the indentation measurements such as nano-porosity, micro-damage, collagencross-links and non-collagenous proteins [62]. In a recent study [52], several cavities such as lacunae were identified below the nanoindentation sites of a mouse femur using FIB-SEM. However, a cavity-free material was found in the majority of the indentation sites.

Finally, the limitation of this work is that the bone tissue was assumed as an homogeneous material, i.e., its microstructure was not accounted for and the viscoelasticity and the anisotropy of the material [6, 25, 46, 74] were not taken into the count in this study. Indeed, the strain rate effect on the mechanical behavior of the cortical bone has not been investigated, since the use of the JC strain rate dependence is required for high-strain-rate deformation of materials. For quasi-static tests, as is the case with the current study, the second factor in the constitutive relationship is neglected. To determine its anisotropic elastic properties, further tests need to be performed along multiple orientations since the cortical bone has a hierarchical and heterogeneous structure. Another limitation of this work is that the sensitivity of the JC material constants to the penetration depth and the indenter geometry was not investigated.

4. Summary and conclusions

- Nanoindentation tests were performed on a cortical bone of a cadaver femur ;
- The experimental results showed that the mechanical response of the material depends on the loading direction and for the same indentation site, a scatter in nanoindentation results was observed ;
- The finite element analysis was used for modeling the nanoindentation testing ;
- The material was considered as work-hardening elastic-plastic material ;

- The JC isotropic hardening model was used to predict the mechanical behavior of the material ;
- The inverse optimization approach was used for determining the unknown material constants from the force-displacement raw data in loading phase, as input data in the optimization process ;
- The predicted elastic constants were determined from the initial elastic contact ;
- The unknown material constants were predicted independently and simultaneously ;
- The predicted values of the yield stress and the elastic constants were in agreement with the existing results in the literature ;
- The numerical curves were well fitted to the target curves ;
- No pile-up of material was predicted around the contact impression by the JC model ;
- The DOE approach was used to investigate the linear effects of the material elastic-plastic constants on the mechanical response of the material ;
- It has been shown that the strain hardening modulus and the strain hardening exponent have the most significant effect on the material response ;
- Finally, the results demonstrated that the JC model can predict accurately the elastoplastic behavior of the cortical bone in nanoindentation.

Conflict of interest statement

None of the authors have any conflicts of interest.

Acknowledgments

This work was supported by QUICKMOLD project.

References

[1] Alam, K., Khan, M., Silberschmidt, V. V., 2014. 3d finite-element modelling of drilling cortical bone: Temperature analysis. J Med Biol Eng 34 (6), 618–23.

[2] Alam, K., Mitrofanov, A., Silberschmidt, V. V., 2009. Finite element analysis of forces of plane cutting of cortical bone. Computational Materials Science 46 (3), 738–743.

[3] Alam, K., Mitrofanov, A., Silberschmidt, V. V., 2010. Thermal analysis of orthogonal cutting of cortical bone using finite element simulations. International Journal of Experimental and Computational Biomechanics 1 (3), 236–251.

[4] Banerjee, A., Dhar, S., Acharyya, S., Datta, D., Nayak, N., 2015. Determination of johnson cook material and failure model constants and numerical modelling of charpy impact test of armour steel. Materials Science and Engineering: A 640, 200–209.

[5] Bayraktar, H. H., Morgan, E. F., Niebur, G. L., Morris, G. E., Wong, E. K., Keaveny, T. M., 2004. Comparison of the elastic and yield properties of human femoral trabecular and cortical bone tissue. Journal of Biomechanics 37 (1), 27–35.

[6] Bekker, A., Kok, S., Cloete, T., Nurick, G., 2014. Introducing objective power law rate dependence into a visco-elastic material model of bovine cortical bone. International Journal of Impact Engineering 66, 28–36.

[7] Bernard, S., Grimal, Q., Laugier, P., 2013. Accurate measurement of cortical bone elasticity tensor with resonant ultrasound spectroscopy. Journal of the Mechanical Behavior of Biomedical Materials 18, 12–19.

[8] Bolshakov, A., Oliver, W., Pharr, G., 1996. Influences of stress on the measurement of mechanical properties using nanoindentation: Part ii. finite element simulations. Journal of Materials Research 11 (3), 760–768.

[9] Bolshakov, A., Pharr, G., 1998. Influences of pileup on the measurement of mechanical properties by load and depth sensing indentation techniques. Journal of Materials Research 13 (4), 1049–1058.

[10] Bushby, A., Ferguson, V., Boyde, A., 2004. Nanoindentation of bone: Comparison of specimens tested in liquid and embedded in polymethylmethacrylate. Journal of Materials Research 19 (1), 249–259.

[11] Callister, W. D., Rethwisch, D. G., 2000. Fundamentals of materials science and engineering. Vol. 471660817. Wiley London.

[12] Carnelli, D., Gastaldi, D., Sassi, V., Contro, R., Ortiz, C., Vena, P., 2010. A finite element model for direction-dependent mechanical response to nanoindentation of cortical bone allowing for anisotropic post-yield behavior of the tissue. Journal of Biomechanical Engineering 132 (8), 081008.

[13] Carnelli, D., Lucchini, R., Ponzoni, M., Contro, R., Vena, P., 2011. Nanoindentation testing and finite element simulations of cortical bone allowing for anisotropic elastic and inelastic mechanical response. Journal of Biomechanics 44 (10), 1852–1858.

[14] Chang, A. C., Liao, J.-D., Liu, B. H., 2016. Practical assessment of nanoscale indentation techniques for the biomechanical properties of biological materials. Mechanics of Materials 98, 11–21.

[15] Chen, Z., Diebels, S., 2012. Nanoindentation of hyperelastic polymer layers at finite deformation and parameter re-identification. Archive of Applied Mechanics 82 (8), 1041–1056.

[16] Chen, Z., Diebels, S., 2013. Parameter re-identification in nanoindentation problems of viscoelastic polymer layers: small deformation. ZAMM-Journal of Applied Mathematics and Mechanics/Zeitschrift für Angewandte Mathematik und Mechanik 93 (2-3), 88–101.

[17] Cowin, S. C., et al., 2001. Bone mechanics handbook. CRC press.

[18] Dey, S., Børvik, T., Hopperstad, O., Langseth, M., 2007. On the influence of constitutive relation in projectile impact of steel plates. International Journal of Impact Engineering 34 (3), 464–486.

[19] Drucker, D. C., Prager, W., 1952. Soil mechanics and plastic analysis or limit design. Quarterly of Applied Mathematics 10 (2), 157–165.

[20] Evans, G., Behiri, J., Currey, J., Bonfield, W., 1990. Microhardness and young's modulus in cortical bone exhibiting a wide range of mineral volume fractions, and in a bone analogue. Journal of Materials Science: Materials in Medicine 1 (1), 38–43.

[21] Faingold, A., Cohen, S. R., Wagner, H. D., 2012. Nanoindentation of osteonal bone lamellae. Journal of the Mechanical Behavior of Biomedical Materials 9, 198–206.

[22] Fan, Z., Rho, J., Swadener, J., 2004. Three-dimensional finite element analysis of the effects of anisotropy on bone mechanical properties measured by nanoindentation. Journal of Materials Research 19 (1), 114–123.

[23] Fan, Z., Rho, J.-Y., 2003. Effects of viscoelasticity and time-dependent plasticity on nanoindentation measurements of human cortical bone. Journal of Biomedical Materials Research Part A 67 (1), 208–214.

[24] Fan, Z., Swadener, J., Rho, J., Roy, M., Pharr, G., 2002. Anisotropic properties of human tibial cortical bone as measured by nanoindentation. Journal of Orthopaedic Research 20 (4), 806–810.

[25] Feng, L., Chittenden, M., Schirer, J., Dickinson, M., Jasiuk, I., 2012. Mechanical properties of porcine femoral cortical bone measured by nanoindentation. Journal of Biomechanics 45 (10), 1775–1782.

[26] Fondrk, M., Bahniuk, E., Davy, D., Michaels, C., 1988. Some viscoplastic characteristics of bovine and human cortical bone. Journal of Biomechanics 21 (8), 623–630.

[27] Franzoso, G., Zysset, P. K., 2009. Elastic anisotropy of human cortical bone secondary osteons measured by nanoindentation. Journal of Biomechanical Engineering 131 (2), 021001.

[28] Ghanbari, J., Naghdabadi, R., 2009. Nonlinear hierarchical multiscale modeling of cortical bone considering its nanoscale microstructure. Journal of Biomechanics 42 (10), 1560–1565.

[29] Giunta, A., Wojtkiewicz, S., Eldred, M., 2003. Overview of modern design of experiments methods for computational simulations. In: 41st Aerospace Sciences Meeting and Exhibit. p. 649.

[30] Hamed, E., Lee, Y., Jasiuk, I., 2010. Multiscale modeling of elastic properties of cortical bone. Acta Mechanica 213, 131–154.

[31] Hamed, E., Novitskaya, E., Li, J., Jasiuk, I., McKittrick, J., 2015. Experimentally-based multiscale model of the elastic moduli of bovine trabecular bone and its constituents. Materials Science and Engineering: C 54, 207–216.

[32] Hay, J. C., Bolshakov, A., Pharr, G., 1999. A critical examination of the fundamental relations used in the analysis of nanoindentation data. Journal of Materials Research 14 (6), 2296–2305.

[33] Hoffler, C. E., Guo, X. E., Zysset, P. K., Goldstein, S. A., 2005. An application of nanoindentation technique to measure bone tissue lamellae properties. Journal of Biomechanical Engineering 127 (7), 1046–1053.

[34] Isaksson, H., Nagao, S., MaŁkiewicz, M., Julkunen, P., Nowak, R., Jurvelin, J. S., 2010. Precision of nanoindentation protocols for measurement of viscoelasticity in cortical and trabecular bone. Journal of Biomechanics 43 (12), 2410–2417.

[35] Jasiuk, I., Ostoja-Starzewski, M., Nov. 2004. Modeling of bone at a single lamella level. Biomechanics and Modeling in Mechanobiology 3, 67–74.

[36] Johnson, G. R., Cook, W. H., 1983. A constitutive model and data for metals subjected to large strains, high strain rates and high temperatures. In: Proceedings of the 7th International Symposium on Ballistics. Vol. 21. The Hague, The Netherlands, pp. 541–547.

[37] Johnson, W. M., Rapoff, A. J., 2003. Characterization of the microindentation of bone via scanning electron microscopy. In: Proceedings of the Summer Bioengineering Conference.

[38] Joo, W., Kim, B., Bae, S. I., Kim, C. S., Song, J. I., 2007. Mechanical properties on nanoindentation measurements of osteonic lamellae in a human cortical bone. In: Key Engineering Materials. Vol. 353. Trans Tech Publ, pp. 2248–2252.

[39] Kang, J., Becker, A. A., Sun, W., 2015. Determination of elastic and viscoplastic material properties obtained from indentation tests using a combined finite element analysis and optimization approach. Proceedings of the Institution of Mechanical Engineers, Part L: Journal of Materials: Design and Applications 229 (3), 175–188.

[40] Lai, Z. B., Yan, C., 2017. Mechanical behaviour of staggered array of mineralised collagen fibrils in protein matrix: Effects of fibril dimensions and failure energy in protein matrix. Journal of the Mechanical Behavior of Biomedical Materials 65, 236–247.

[41] Lang, S. B., 1969. Elastic coefficients of animal bone. Science 165 (3890), 287–288.

[42] Milani, A., Dabboussi, W., Nemes, J., Abeyaratne, R., 2009. An improved multi-objective identification of johnson–cook material parameters. International Journal of Impact Engineering 36 (2), 294–302.

[43] Mullins, L., Bruzzi, M., McHugh, P., 2009. Calibration of a constitutive model for the post-yield behaviour of cortical bone. Journal of the Mechanical Behavior of Biomedical Materials 2 (5), 460–470.

[44] Nocedal, Jorge; Wright, S. J., 2006. [Springer Series in Operations Research and Financial Engineering] Numerical Optimization.

[45] Öchsner, A., Ahmed, W., 2011. Biomechanics of hard tissues. John Wiley & Sons.

[46] Olesiak, S. E., Oyen, M. L., Ferguson, V. L., 2010. Viscous-elastic-plastic behavior of bone using berkovich nanoindentation. Mechanics of Time-Dependent Materials 14 (2), 111–124.

[47] Oliver, W. C., Pharr, G. M., 1992. An improved technique for determining hardness and elastic modulus using load and displacement sensing indentation experiments. Journal of Materials

Research 7 (6), 1564–1583.

[48] Oliver, W. C., Pharr, G. M., 2004. Measurement of hardness and elastic modulus by instrumented indentation: Advances in understanding and refinements to methodology. Journal of Materials Research 19 (1), 3–20.

[49] Peterson, D. R., Bronzino, J. D., 2007. Biomechanics: principles and applications. CRC press.

[50] Poon, B., Rittel, D., Ravichandran, G., 2008. An analysis of nanoindentation in linearly elastic solids. International Journal of Solids and Structures 45 (24), 6018–6033.

[51] Porter, D., 2004. Pragmatic multiscale modelling of bone as a natural hybrid nanocomposite. Materials Science and Engineering: A 365 (1), 38–45.

[52] Ramezanzadehkoldeh, M., Skallerud, B., 2017. Nanoindentation response of cortical bone: dependency of subsurface voids. Biomechanics and modeling in mechanobiology 16 (5), 1599–1612.

[53] Reisinger, A. G., Pahr, D. H., Zysset, P. K., 2011. Principal stiffness orientation and degree of anisotropy of human osteons based on nanoindentation in three distinct planes. Journal of the Mechanical Behavior of Biomedical Materials 4 (8), 2113–2127.

[54] Rho, J., Zioupos, P., Currey, J., Pharr, G., 1999. Variations in the individual thick lamellar properties within osteons by nanoindentation. Bone 25 (3), 295–300.

[55] Rho, J.-Y., Roy, M. E., Tsui, T. Y., Pharr, G. M., 1999. Elastic properties of microstructural components of human bone tissue as measured by nanoindentation. Journal of Biomedical Materials Research 45 (1), 48–54.

[56] Rho, J.-Y., Tsui, T. Y., Pharr, G. M., 1997. Elastic properties of human cortical and trabecular lamellar bone measured by nanoindentation. Biomaterials 18 (20), 1325–1330.

[57] Ridha Hambli, Nour Hattab (auth.), A. G. e., 2013. Multiscale Computer Modeling in Biomechanics and Biomedical Engineering, 1st Edition. Studies in Mechanobiology, Tissue Engineering and Biomaterials 14. Springer-Verlag Berlin Heidelberg.

[58] Rodriguez-Florez, N., Oyen, M. L., Shefelbine, S. J., 2013. Insight into differences in nanoindentation properties of bone. Journal of the Mechanical Behavior of Biomedical Materials 18, 90–99.

[59] Schwiedrzik, J., Raghavan, R., Bürki, A., LeNader, V., Wolfram, U., Michler, J., Zysset, P., 2014. In situ micropillar compression reveals superior strength and ductility but an absence of damage in lamellar bone. Nature materials 13 (7), 740.

[60] Schwiedrzik, J. J., Wolfram, U., Zysset, P., 2013. A generalized anisotropic quadric yield criterion and its application to bone tissue at multiple length scales. Biomechanics and modeling in mechanobiology 12 (6), 1155–1168.

[61] Schwiedrzik, J. J., Zysset, P., 2015. Quantitative analysis of imprint shape and its relation to mechanical properties measured by microindentation in bone. Journal of Biomechanics 48 (2), 210–216.

[62] Spiesz, E. M., Reisinger, A. G., Kaminsky, W., Roschger, P., Pahr, D. H., Zysset, P. K., 2013. Computational and experimental methodology for site-matched investigations of the influence of mineral mass fraction and collagen orientation on the axial indentation modulus of lamellar bone. Journal of the Mechanical Behavior of Biomedical Materials 28, 195–205.

[63] Spiesz, E. M., Roschger, P., Zysset, P. K., 2012. Elastic anisotropy of uniaxial mineralized collagen fibers measured using two-directional indentation. effects of hydration state and indentation depth. Journal of the Mechanical Behavior of Biomedical Materials 12, 20–28.

[64] Swadener, J., Rho, J.-Y., Pharr, G., 2001. Effects of anisotropy on elastic moduli measured by nanoindentation in human tibial cortical bone. Journal of Biomedical Materials Research Part A 57 (1), 108–112.

[65] Szabó, M., Thurner, P. J., 2013. Anisotropy of bovine cortical bone tissue damage properties. Journal of biomechanics 46 (1), 2–6.

[66] Tai, K., Ulm, F.-J., Ortiz, C., 2006. Nanogranular origins of the strength of bone. Nano letters 6 (11), 2520–2525.

[67] Tanco, M., Viles, E., Ilzarbe, L., Alvarez, M. J., 2009. Implementation of design of experiments projects in industry. Applied Stochastic Models in Business and Industry 25 (4), 478–505.

[68] Van Buskirk, W., Ashman, R., 1981. The elastic moduli of bone. Mechanical properties of bone 45, 131–143.

[69] Vanleene, M., Mazeran, P.-E., Ho Ba Tho, M.-C., 2007. Influence of nanoindentation test direction on the elastic properties of human cortical bone lamellae. Computer Methods in Biomechanics and Biomedical Engineering 10 (sup1), 127–128.

[70] Vercher-Martinez, A., Giner, E., Arango, C., Fuenmayor, F. J., 2015. Influence of the mineral staggering on the elastic properties of the mineralized collagen fibril in lamellar bone. Journal of the Mechanical Behavior of Biomedical Materials 42, 243 – 256.

[71] Viswanath, B., Raghavan, R., Ramamurty, U., Ravishankar, N., 2007. Mechanical properties and anisotropy in hydroxyapatite single crystals. Scripta Materialia 57 (4), 361–364.

[72] Wang, X., Chen, X., Hodgson, P., Wen, C., 2006. Elastic modulus and hardness of cortical and trabecular bovine bone measured by nanoindentation. Transactions of nonferrous metals society of china 16, s744–s748.

[73] Yoon, Y. J., Cowin, S. C., Feb. 2008. The estimated elastic constants for a single bone osteonal lamella. Biomechanics and Modeling in Mechanobiology 7, 1–11.

[74] Zhang, J., Niebur, G. L., Ovaert, T. C., 2008. Mechanical property determination of bone through nano-and micro-indentation testing and finite element simulation. Journal of Biomechanics 41 (2), 267–275.

[75] Zhang, Y., Outeiro, J., Mabrouki, T., 2015. On the selection of johnson-cook constitutive model parameters for ti-6al-4v using three types of numerical models of orthogonal cutting. Procedia CIRP 31, 112–117.

[76] Zysset, P., Curnier, A., 1995. An alternative model for anisotropic elasticity based on fabric tensors. Mechanics of Materials 21, 243–250.

[77] Zysset, P. K., Guo, X. E., Hoffler, C. E., Moore, K. E., Goldstein, S. A., 1999. Elastic modulus and hardness of cortical and trabecular bone lamellae measured by nanoindentation in the human femur. Journal of Biomechanics 32 (10), 1005–1012.

Fig. 1: Optical microscopy image of human cortical bone obtained from a cadaver femur.

Fig. 2: Boundary conditions of the two-dimensional axisymmetric finite element model simulating the Berkovich indentation test. The reference point (RP) was fixed in the horizontal directions. The nodes at the bottom of the sample part were constrained in all directions, while those at the axis of symmetry were constrained in the horizontal directions. The incremental experimental force as a function of time was applied at the reference point.

Fig. 3: Optimization process diagram.

Fig. 4: The force-displacement curves corresponding to the maximum depth (a) and the minimum depth (b) of the indenter tip for the axial and transverse directions.

Fig. 5: Loading curves obtained from nanoindentation testing performed on the interstitial bone. Eight indents were performed.

Fig. 6: Representative fit between experiment and JC model of a nanoindentation test performed on the interstitial lamellae of a cortical bone sample.

Fig. 7: Finite element modeling of the nanoindentation test performed on a cortical bone. The contour map of the equivalent plastic strain (PEEQ) corresponds to the maximum indenter depth.

Fig. 8: Illustration of Poisson's ratio effect on the nanoindentation results of a cortical bone.

Fig. 9: A Design Of Experiments (DOE) was performed to evaluate the linear effects of the elastic-plastic Johnson–Cook constants on the mechanical response (here, the maximum equivalent stress) of a cortical bone to nanoindentation. The linear effect is evaluated by calculating the averaged responses at the lower and upper bounds of each constant fixed in the optimization process, and then plotted by drawing a straight line between the two average values. The difference between the two average values, that is the linear effect value, is indicated in the legend. For each material constant, the linear effect is calculated for 32 runs of the full factorial DOE. A positive slope indicates a positive effect.

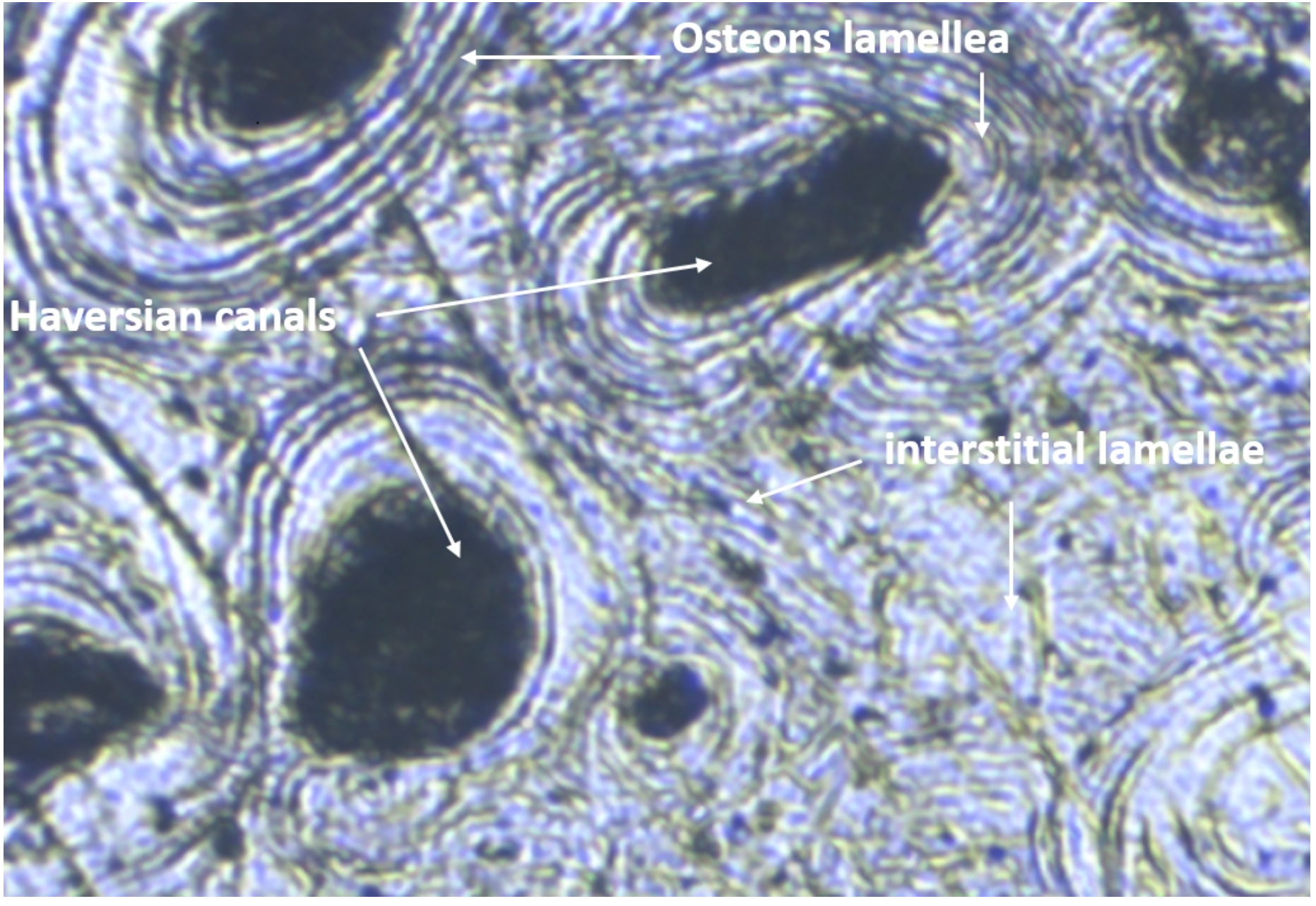
Osteons lamellea
Haversian canals
interstitial lamellae

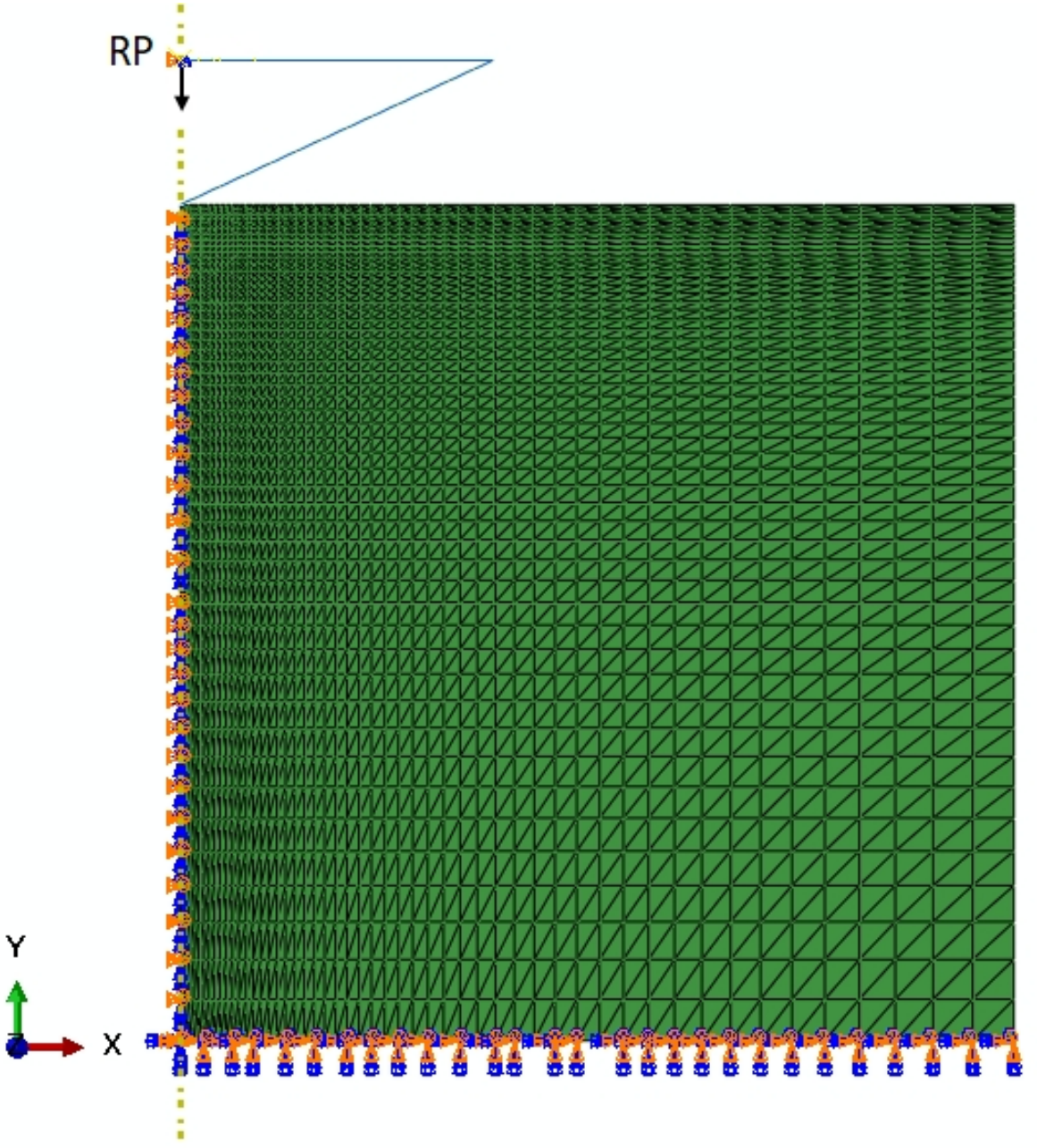
RP
Y
X

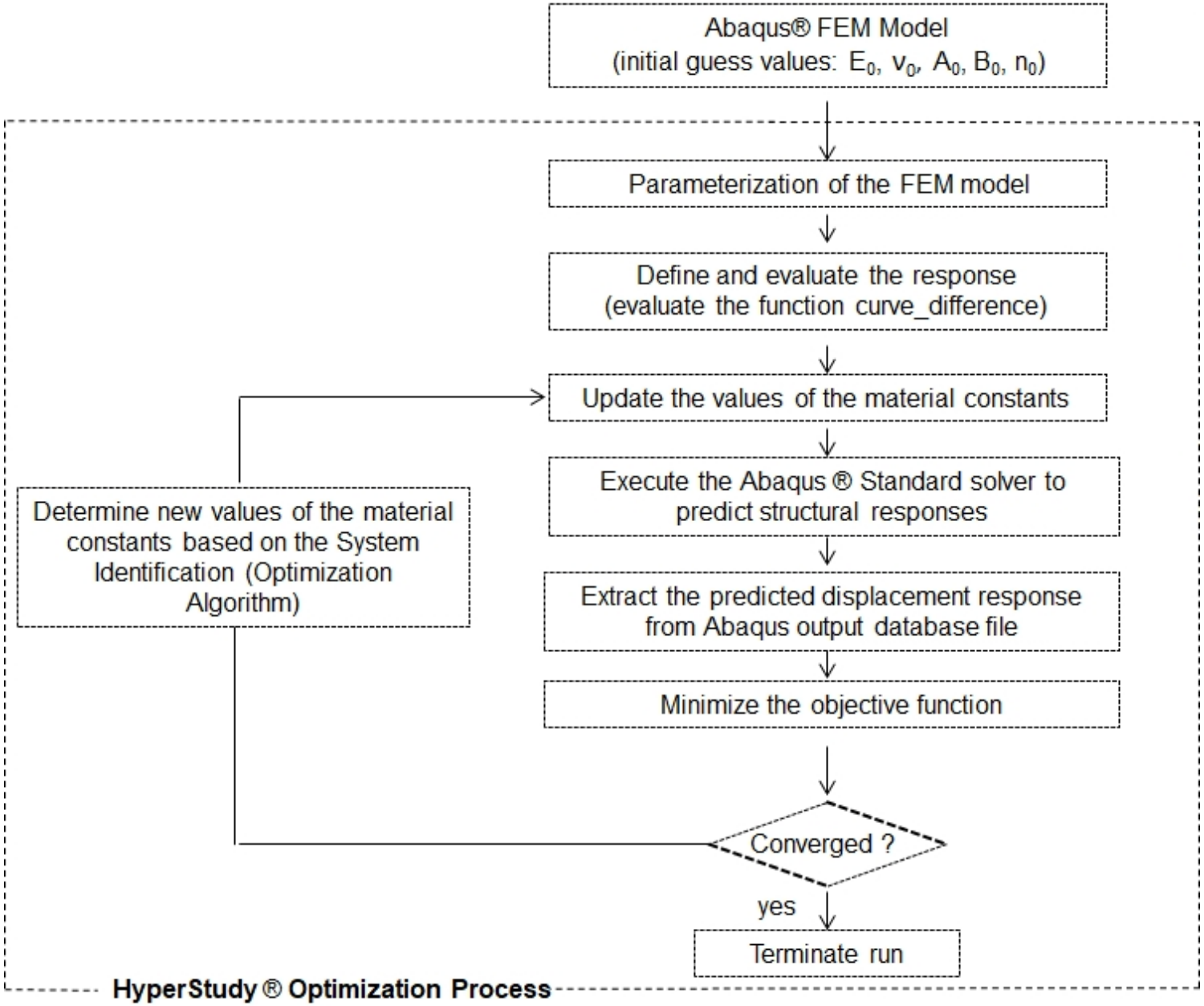
Abaqus® FEM Model
(initial guess values: E_0, ν_0, A_0, B_0, n_0)
Parameterization of the FEM model
Define and evaluate the response
(evaluate the function curve_difference)
Update the values of the material constants
Execute the Abaqus ® Standard solver to predict structural responses
Extract the predicted displacement response from Abaqus output database file
Minimize the objective function
Converged ?
yes
Terminate run
Determine new values of the material constants based on the System Identification (Optimization Algorithm)
HyperStudy ® Optimization Process

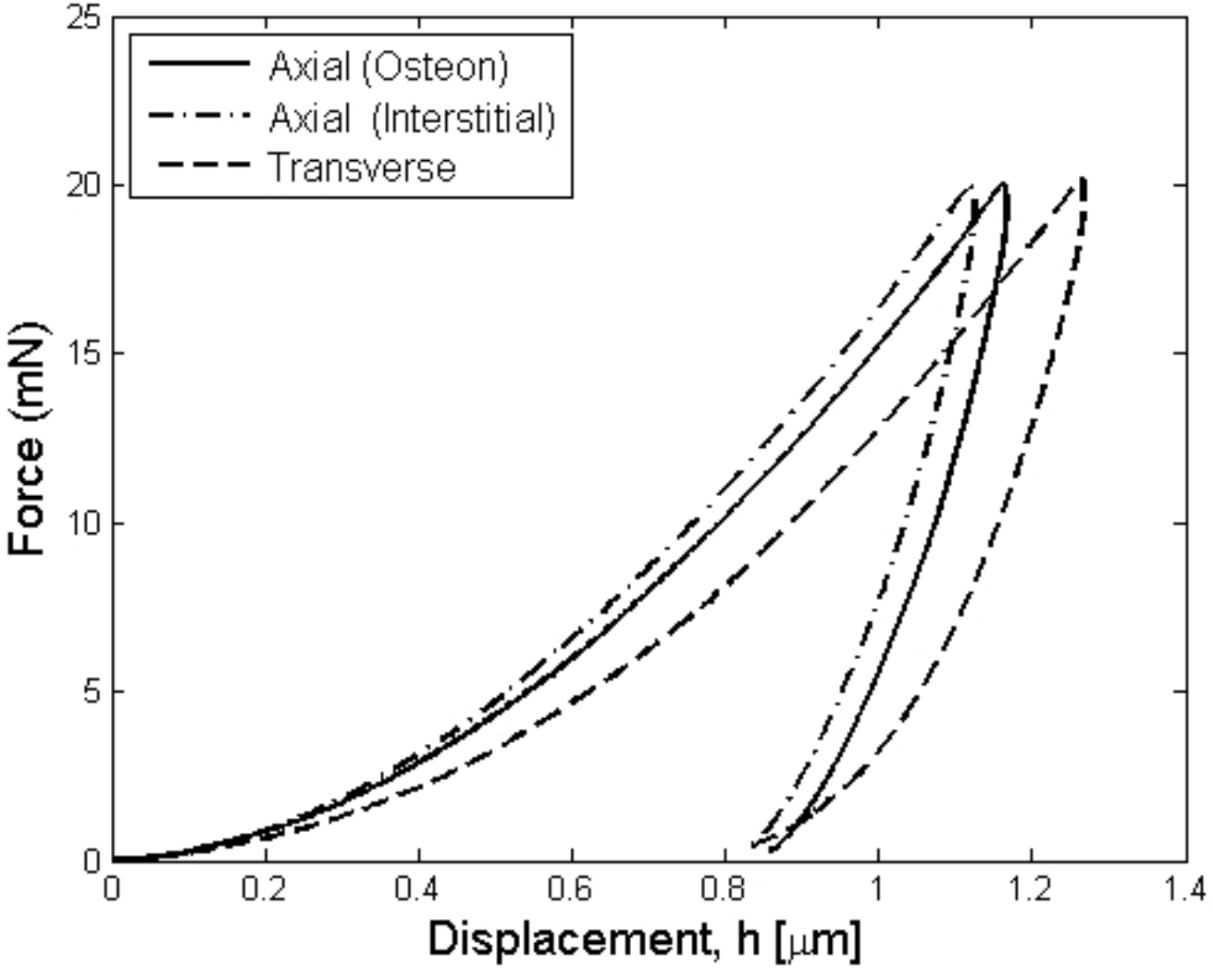
Axial (Osteon)
Axial (Interstitial)
Transverse
Force (mN)
Displacement, h [μm]
0
5
10
15
20
25
0
0.2
0.4
0.6
0.8
1
1.2
1.4

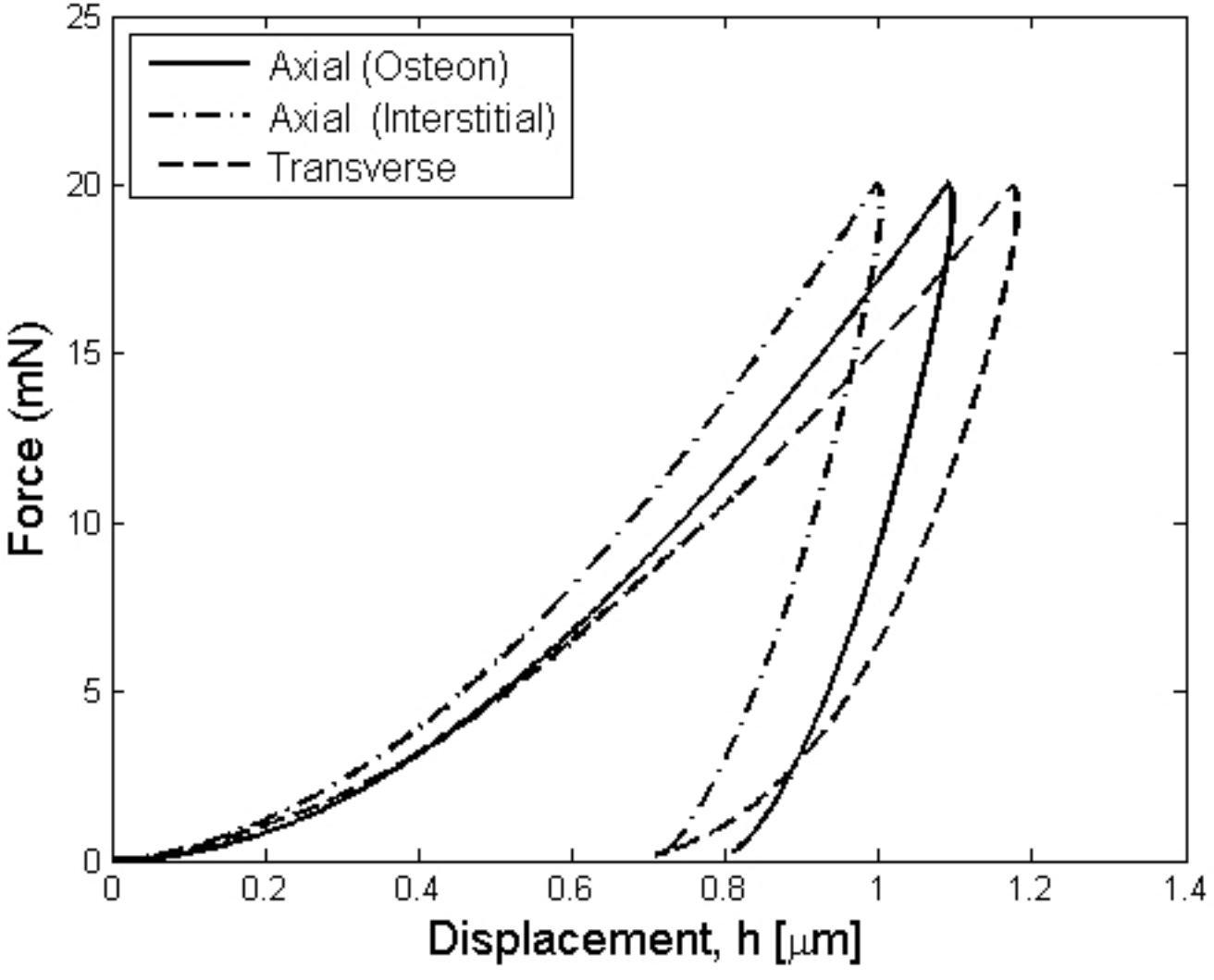
Axial (Osteon)
Axial (Interstitial)
Transverse
Force (mN)
Displacement, h [μm]
0
5
10
15
20
25
0
0.2
0.4
0.6
0.8
1
1.2
1.4

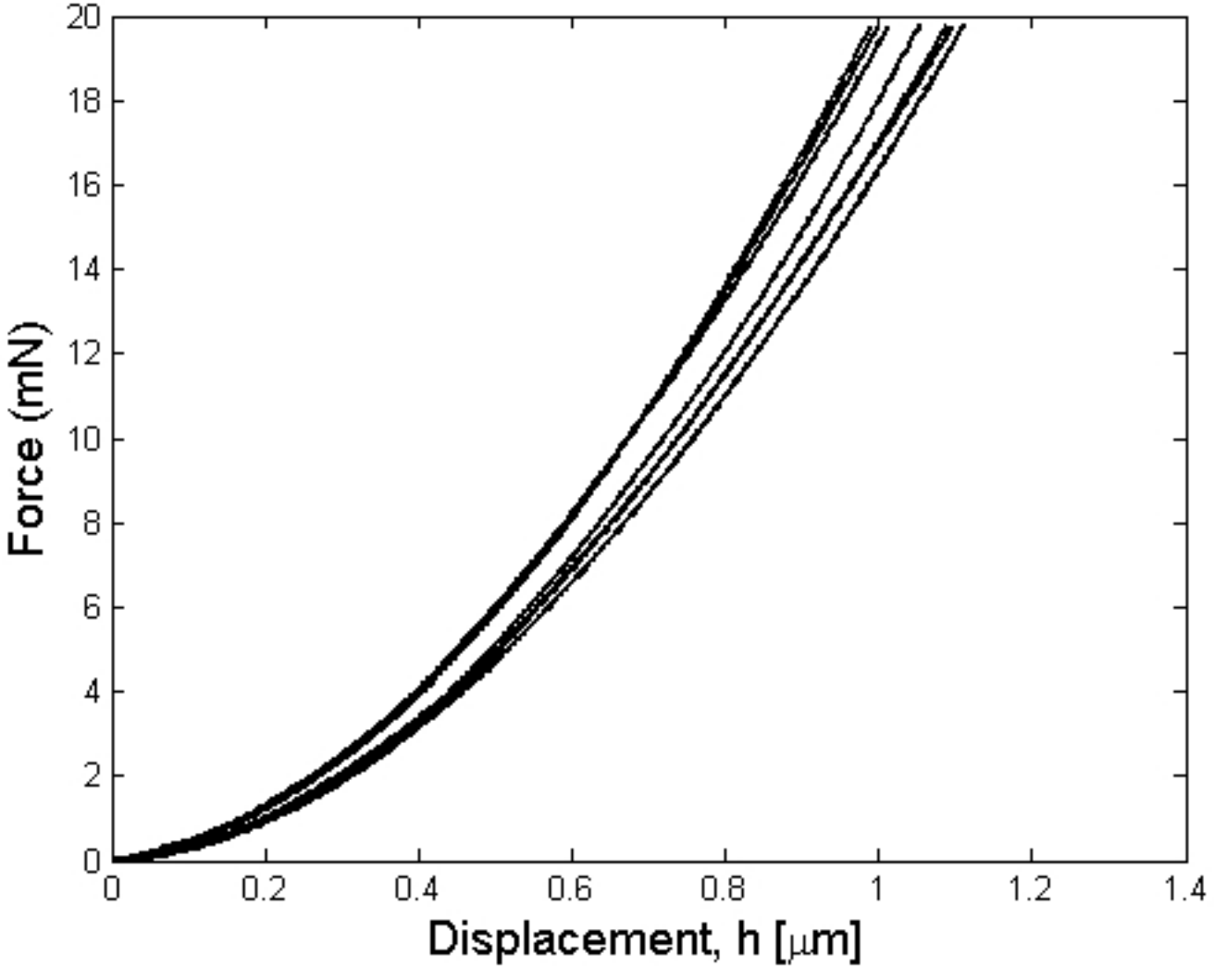
Force (mN)
Displacement, h [μm]
0
2
4
6
8
10
12
14
16
18
20
0
0.2
0.4
0.6
0.8
1
1.2
1.4

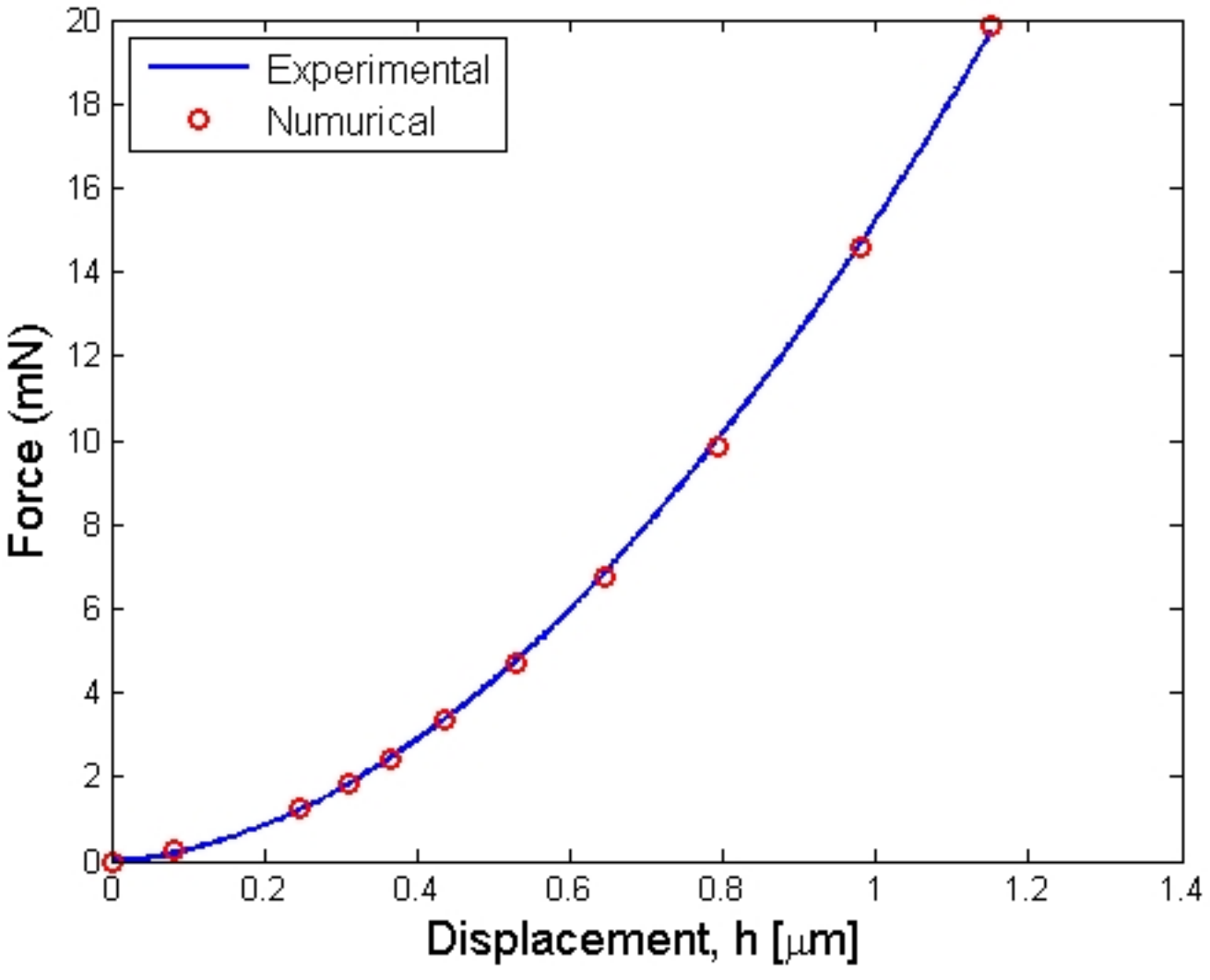
Experimental
Numurical
Force (mN)
Displacement, h [μm]
0
2
4
6
8
10
12
14
16
18
20
0
0.2
0.4
0.6
0.8
1
1.2
1.4

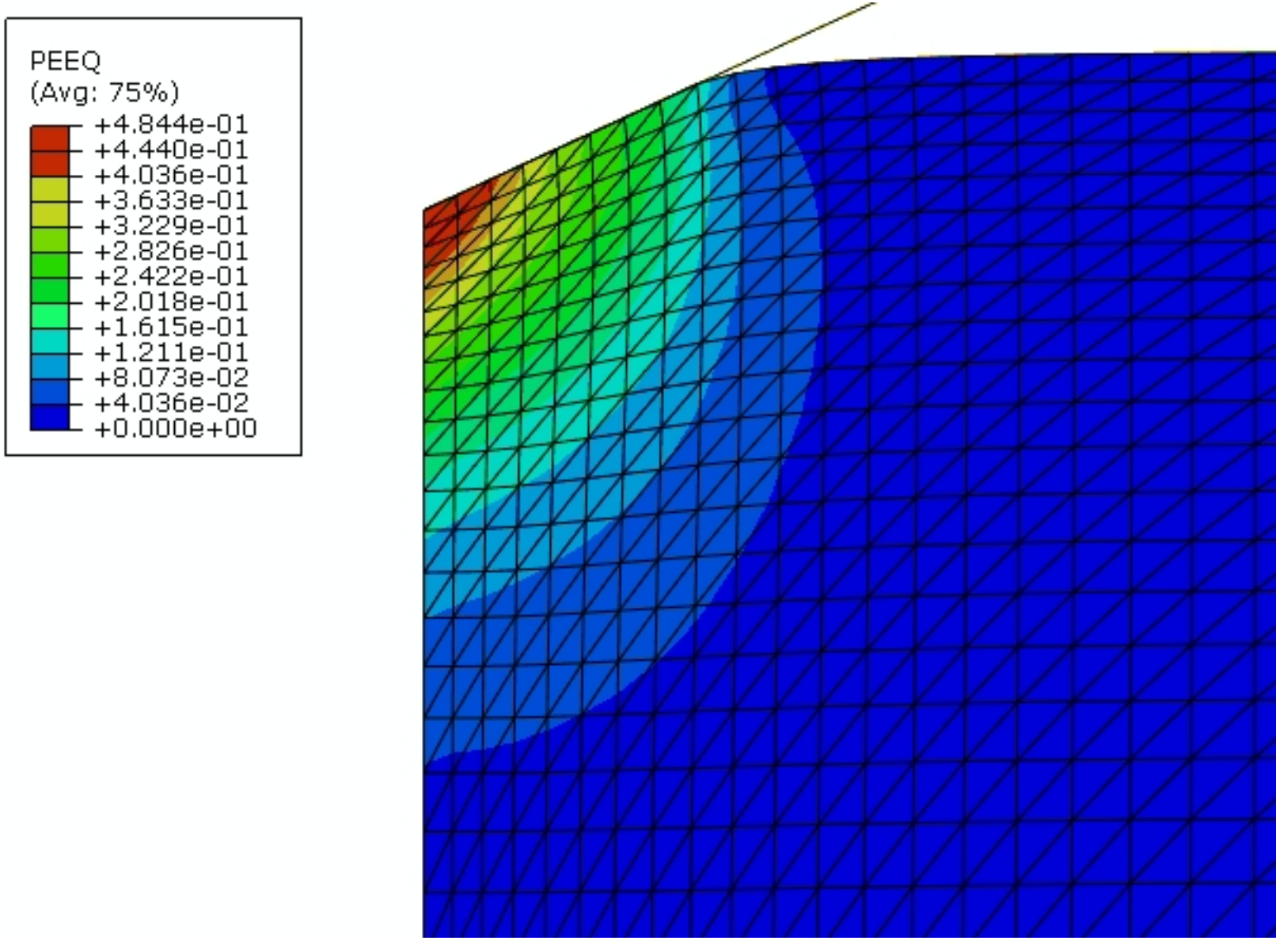
PEEQ
(Avg: 75%)
+4.844e-01
+4.440e-01
+4.036e-01
+3.633e-01
+3.229e-01
+2.826e-01
+2.422e-01
+2.018e-01
+1.615e-01
+1.211e-01
+8.073e-02
+4.036e-02
+0.000e+00

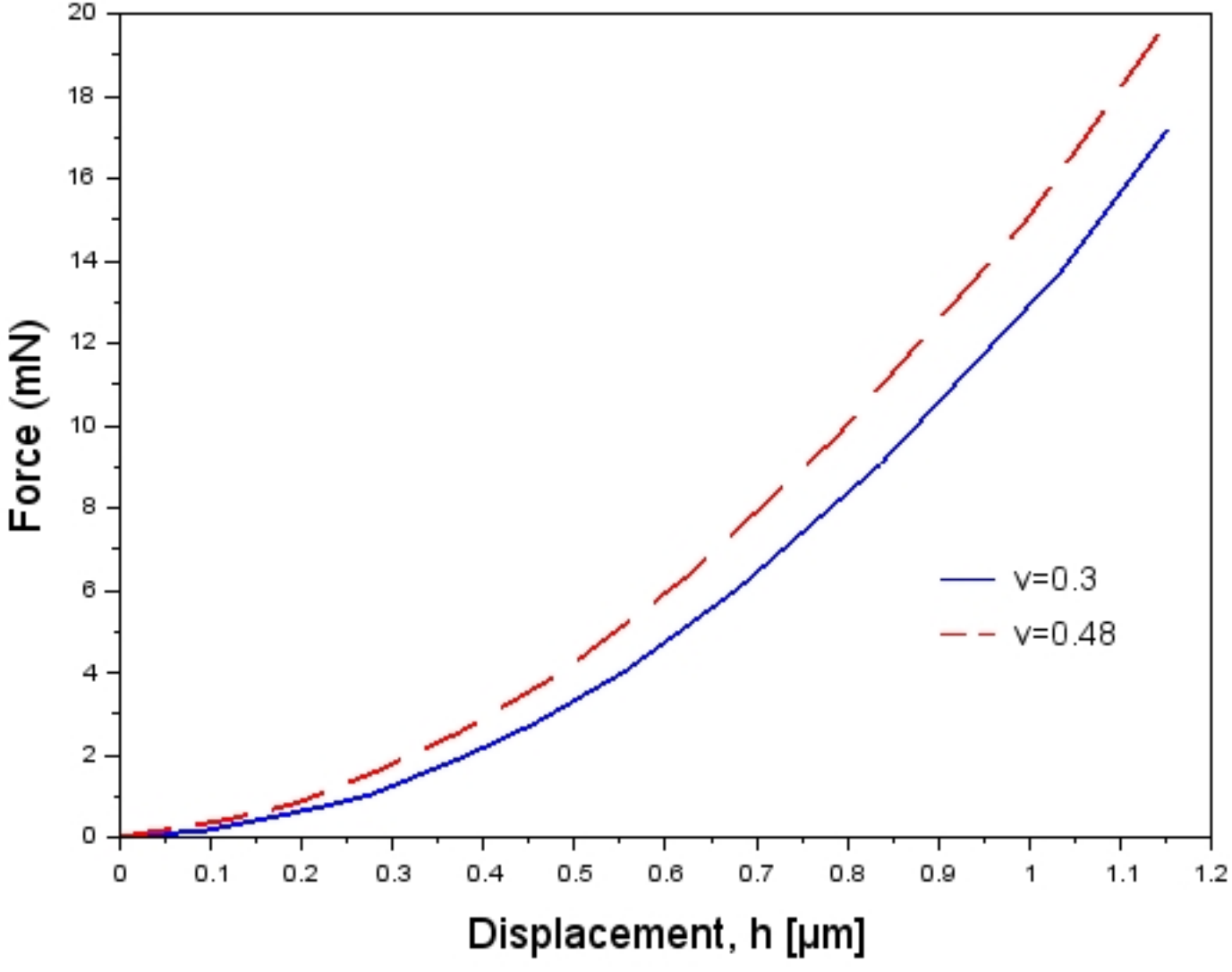
Force (mN)
Displacement, h [μm]
ν=0.3
ν=0.48
0
2
4
6
8
10
12
14
16
18
20
0
0.1
0.2
0.3
0.4
0.5
0.6
0.7
0.8
0.9
1
1.1
1.2

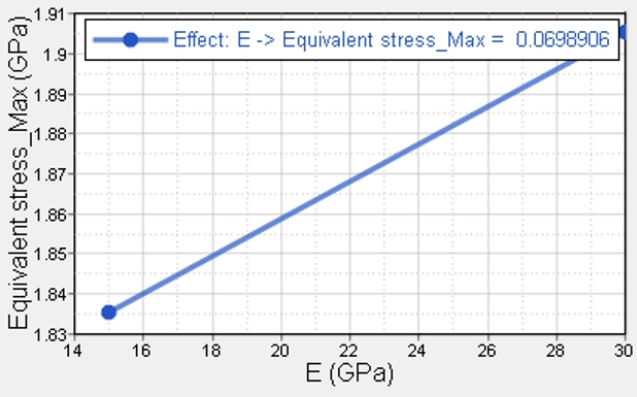
Effect: E -> Equivalent stress_Max = 0.0698906
Equivalent stress_Max (GPa)
E (GPa)

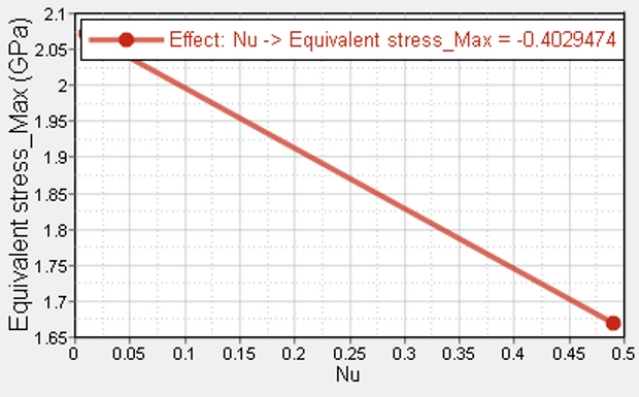
Effect: Nu -> Equivalent stress_Max = -0.4029474
Equivalent stress_Max (GPa)
Nu

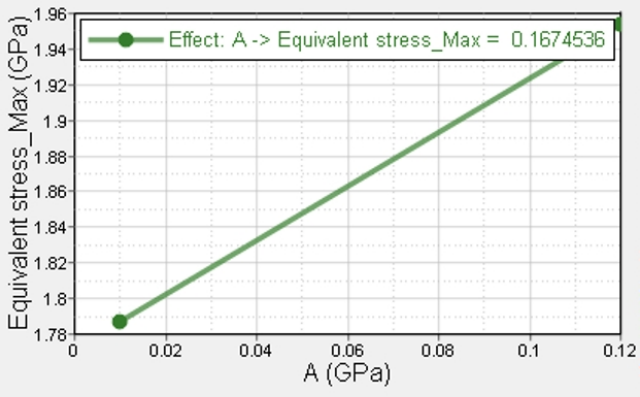
Effect: A -> Equivalent stress_Max = 0.1674536
Equivalent stress_Max (GPa)
A (GPa)

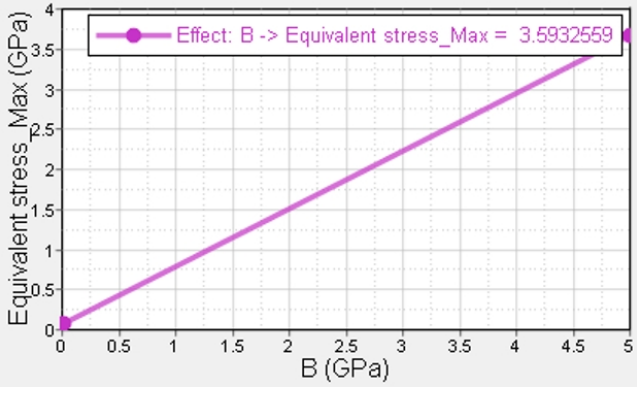
Effect: B -> Equivalent stress_Max = 3.5932559
Equivalent stress_Max (GPa)
B (GPa)


Effect: n -> Equivalent stress_Max = -1.3438942
Equivalent stress_Max (GPa)
n